Chapter 1

Wavefront Reconstruction and Control

Marcos A. van Dam
Flat Wavefronts, 21 Lascelles Street, Christchurch 8022, New Zealand
marcos@flatwavefronts.com

Wavefront sensors typically measure a derivative of the wavefront. In this chapter we address two important problems: how to convert these wavefront derivatives into wavefront estimates, and how to use these wavefront estimates to drive the deformable mirrors.

1. Introduction

Wavefront sensors (WFSs) in astronomical adaptive optics (AO) typically measure a derivative of the wavefront. The Shack-Hartmann (SH) WFS and the modulated pyramid WFS both measure the x- and y-slopes, while the curvature WFS measures the Laplacian of the wavefront. In this chapter we address two important problems: wavefront reconstruction and wavefront control. Wavefront reconstruction deals with the problem of converting wavefront derivatives into wavefront estimates, while wavefront control deals with how to use these wavefront estimates to drive the deformable mirrors (DMs).

Without loss of generality, in this chapter we often assume that the WFS is of a Shack-Hartmann type, with square subapertures and with a linear response to the incoming wavefront. The DM has a square array of actuators with the same geometry as the WFS. The actuators are optically conjugate to the corners of the lenslet array in what is commonly known as the Fried configuration. The DMs also respond linearly to the applied command.

Most AO systems use closed-loop control, where the wavefront sensor is located after the DM. Thus, the WFS measures the corrected wavefront. In open-loop control, the wavefront sensor is located before the DM, and does not see the correction applied by the DM. In so-called pseudo open-loop control, we convert the closed-loop measurements into open-loop measurements by adding the contribution from the applied DM commands. The wavefront reconstruction strategy depends on whether we use closed-loop or open-loop measurements.

2. Interaction matrix

The interaction matrix, G_a describes how the vector representing the DM command, $\mathbf{a}$, affects the WFS measurement vector, $\mathbf{s}$:

$$\mathbf{s} = G_a \mathbf{a}. \tag{1}$$

The interaction matrix incorporates the details about the behavior of the WFS and of the DM and is needed to compute the reconstructor. The simplest way to measure it is to poke the actuators one by one by increment d. The poke increment is a free parameter but should be chosen to be as large as possible to maximize the signal-to-noise ratio (SNR) while keeping both the WFS and the DM actuators within their linear range. We create a matrix of poked actuators, $A = [\mathbf{a_1}, \mathbf{a_2}, \mathbf{a_3}, ...]$, where $\mathbf{a_1}^T = [d, 0, 0, ...]$, $\mathbf{a_2}^T = [0, d, 0, 0, ...]$, *etc.* In this case, $A = dI$, where I is the identity matrix. The corresponding matrix of measurements, S is similarly comprised of $S = [\mathbf{s_1}, \mathbf{s_2}, \mathbf{s_3}, ...]$. Using the relationship

$$S = G_a A, \tag{2}$$

we see that

$$\begin{aligned} G_a &= SA^{-1} \\ &= S(dI)^{-1} \\ &= d^{-1}S. \end{aligned} \tag{3}$$

This simple method works well when there is an accurate way to measure the change in centroids to the applied commands (*e.g.*, using a calibration source). However, the method is noisy since subapertures far away from the applied actuator are only measuring noise. The measurements from those subapertures should be masked.

The actuators do not need to be poked one by one: instead, we can use any orthogonal set of pokes. By careful selection of the set of commands, we can greatly improve the SNR. An ideal choice is the Walsh basis set.[1,2]

There are some AO systems, notably those that employ adaptive secondary mirrors, where calibration of the interaction matrix in controlled conditions is difficult or impossible. In this case, we are forced to calibrate the interaction matrix using starlight. Poking actuators one by one is not a good solution since the measurements are affected by atmospheric turbulence. Instead, we create mirror modes (some possible basis sets are described in Section 3.3). Each mirror mode is associated with a time-varying sinusoid at a high temporal frequency (typically 50 Hz or higher), at which we do not expect to find much power in the atmospheric turbulence. The effect of each mode is demodulated from the recorded WFS measurements.[3,4] The reader is referred to Esposito *et al* for more details.[3]

All of these methods for generating interaction matrices work when there are multiple guide stars and/or DMs.

3. Classical reconstructors

The term classical reconstructors is used here to describe reconstructors that are a regularized inverse of the interaction matrix. In most cases, the wavefront reconstruction is implemented by multiplying a reconstructor matrix, R, by a vector of measurements, s, to obtain the residual wavefront, $\mathbf{a}$, in actuator space:

$$\mathbf{a} = R\mathbf{s}. \tag{4}$$

In general, G_a is not a square matrix so it cannot be inverted. We could define the reconstructor as the pseudo-inverse of G_a:

$$R = ({G_a}^T G_a)^{-1} {G_a}^T. \tag{5}$$

However, ${G_a}^T G_a$ is not invertible. Instead, the reconstructor is a *regularized* pseudo-inverse of G_a. How to regularize the matrix inversion is the subject of this section. There is a fundamental trade-off between reconstructing the wavefront to cancel the centroids as much as possible on one hand, and reducing the effect of noise in the centroids on the wavefront reconstruction. Even if the guide star is extremely bright, the centroid measurements are contaminated by noise stemming from spatial aliasing[5] and truncation of the detector area.[6]

Three different ways to compute classical reconstructors are discussed in this section: singular value decomposition, regularized least-squares and modal reconstructors. These reconstructors, which comprise almost all existing reconstructors in astronomical AO, drive the DM actuators to make the WFS measurements as close as possible to zero (or to the calibrated reference values of the WFSs). The reconstructors may incorporate knowledge of the location of the guide star(s) and the statistics of the turbulence and noise.

Tomographic reconstructors on the other hand, use measurements from several guide stars to drive the actuators to compensate the wavefront optimally in the direction of the science targets (not the WFSs). Tomographic reconstructors, which are the subject of Section 4, can also incorporate knowledge of the location of the science target(s) and the strength of the turbulent layers.

For computational reasons, AO systems with large numbers of measurements or actuators may need to reconstruct the wavefront using alternative approaches to reconstruction matrices. Some of these approaches are discussed in Section 5.

3.1. *Singular value decomposition*

The traditional way to compute R is to take a singular value decomposition (SVD) of G_a. The SVD reconstructor is still used for small scale AO systems and for AO systems where the sampling of the WFS is denser than the interactuator spacing. The attraction of the SVD reconstructor is that it takes the interaction matrix and the number of modes (or minimum singular value) as the only inputs.

Let us decompose the matrix G_a using the SVD:

$$G_a = UDV^T, \tag{6}$$

where U and V are unitary matrices representing the singular modes of the WFS and the DM respectively. D is a diagonal matrix, with the values along the leading diagonal known as singular values.

Recall that a unitary matrix has the property that its inverse is equal to its transpose. Hence, the pseudo-inverse, G_a^+, is:

$$G_a^+ = VD^{-1}U^T. \tag{7}$$

The reconstructor is a regularized pseudo-inverse obtained by inverting only the largest singular values. For example, to keep the first m singular modes, we define D^{-1} as:

$$D_{ii}^{-1} = \begin{cases} 1/D_{ii}, & \text{if } i <= m \\ 0, & \text{otherwise.} \end{cases} \tag{8}$$

The number of modes to keep (or, alternatively, the smallest singular value to invert) is a free parameter. At a minimum, invisible modes such as pure actuator piston or global waffle must be removed. The optimal number of modes depends on the signal-to-noise ratio of the WFS and is generally determined via numerical simulations and/or on-sky performance testing. Fig. 1 illustrates two modes with low singular values. The disadvantage of the SVD reconstructor is that each mode

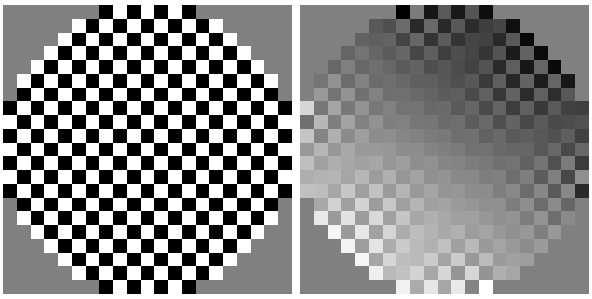

Fig. 1. Global waffle mode on the DM (left) and a mode containing partial waffle (right). These modes are not well sensed by a Shack-Hartmann WFS and must be removed in the reconstruction process.

(which comprises a vector of actuator commands) is either kept intact or discarded entirely, leading to lower performance. The SVD process also imposes a heavy computational burden which can be prohibitive for systems with a large number of actuators.

3.2. *Regularized least-squares reconstructors*

Most current astronomical AO systems use some form of regularized least-squares reconstruction.[4,7–9] A regularized least-squares reconstructor takes the form:

$$R = ({G_a}^T W G_a + Q)^{-1} {G_a}^T W, \tag{9}$$

where W is a diagonal matrix that weights the measurements differently and may be omitted if all measurements are equally noisy or the noise is unknown. Examples where W is useful are: SH WFSs where some subapertures are only partially illuminated, curvature WFS with different size subapertures, and any WFS guiding on a laser guide star (LGS), where the elongation of the guide star depends on the location of the pupil.[10] The matrix ${G_a}^T W G_a$ is not invertible for the same reason that some of the singular values in the SVD are very small: some mirror modes are unsensed or poorly sensed by the WFS. Hence, a regularization matrix Q is needed to make the system of equations well conditioned.

The simplest form of regularization is

$$Q = \alpha I, \tag{10}$$

where I is the identity matrix and α is a constant. The optimal value of α is found by trial and error and increases with increasing measurement noise. This form of regularization penalizes all of the actuator commands equally. However, the mirror modes are not penalized equally: it can be shown that this reconstructor is exactly the same as the SVD reconstructor where the diagonal matrix of Eq. (8) is replaced by:

$$D_{ii}^{-1} = \frac{1}{\alpha + D_{ii}}. \tag{11}$$

This means that mirror modes with a low singular value suffer much stronger penalization than modes which are well measured and hence have a high singular value.

We can also set Q explicitly to penalize unwanted modes. For example, piston can be removed using extremely strong penalization by setting

$$Q = \beta \mathbf{p}\mathbf{p}^T, \tag{12}$$

where $\mathbf{p}^T = [1, 1, \cdots]$ and β is a large constant. In the same way, we can penalize other unwanted modes, such as tip-tilt for AO systems with a separate tip-tilt mirror. Local waffle, which is prevalent in SH WFSs, can be penalized using a local waffle supressing matrix Q.[7] Alternatively, we can use prior knowledge that atmospheric turbulence is smooth and use Laplacian penalization, a very sparse matrix Q which penalizes the curvature of the wavefront.[11]

Finally, let us consider the minimum-variance estimator (also known as the minimum mean squared error estimator).[12] This reconstructor minimizes the wavefront error when running in open loop. There are different, mathematically equivalent, ways of writing this:

$$\begin{aligned} R &= C_{as} C_{ss}^{-1} && (13)\\ &= C_{aa} {G_a}^T (G_a C_{aa} {G_a}^T + C_{nn})^{-1} && (14)\\ &= ({G_a}^T C_{nn}^{-1} G_a + C_{aa}^{-1})^{-1} {G_a}^T C_{nn}^{-1} && (15) \end{aligned}$$

where C_{nn} is the covariance of the measurement noise and C_{aa} is the covariance of atmospheric turbulence in actuator space (*i.e.*, the covariance of the actuators commands in the absence of noise).

The matrix

$$C_{as} = C_{aa} {G_a}^T \tag{16}$$

represents the covariance between the measurement and the turbulence, while

$$C_{ss} = G_a^T C_{aa} {G_a}^T + C_{nn} \tag{17}$$

is the covariance of the measurements.

We can calculate the matrix C_{nn}, analytically or using Monte-Carlo simulations, based on the brightness of the star and the noise characteristics of the detector. Alternatively, C_{nn} can be measured on the sky. The calculation C_{aa} is described in Section 4.3.

In practice, most AO systems run in closed-loop, where the measurements correspond to the residual wavefront errors, not the wavefront itself. The reconstructor becomes:

$$R = ({G_a}^T C_{nn}^{-1} G_a + \alpha C_{aa}^{-1})^{-1} {G_a}^T C_{nn}^{-1}, \tag{18}$$

where α is a small constant tuned to the signal-to-noise of the WFS. This reconstructor is used at Keck Observatory and on GeMS.[4,8]

3.3. *Modal reconstructors*

In many cases, we wish to convert from wavefront derivative measurements to a set of global modes before converting to actuator commands. The most commonly used modes in astronomical adaptive optics are the Zernike,[13] Karhunen-Loève[14] (KL), disk harmonics[15] and Fourier[16,17] basis sets. The attractive properties of each modal basis function are described in what follows.

Zernike modes are popular as they correspond to physical optical quantities, such as piston, tip-tilt, focus and astigmatism. There is a simple analytical expression for the modes and their for derivatives over a circular pupil. Their use should be restricted to about 45 modes, after which the modes exhibit large derivatives near the edge of the pupil.

KL modes are the eigenmodes of atmospheric turbulence (*i.e.*, the eigenmodes of C_{aa}) and by definition can be used to measure or compensate the largest fraction of turbulence using a given number of modes. Disadvantages of KL modes are the difficulty in computing them and the fact that they have no physical meaning.

Disk harmonics are similar to Zernike modes, but are much better behaved near the edges. Adaptive secondary mirrors, which have a large number of modes over a circular pupil, are usually commanded in disk harmonics or KL modes.

Fourier modes are orthogonal over a rectangular aperture, and are ideally suited to WFSs with measurements in a grid and DMs with a rectangular array of actuators. The modes are perfect for describing wavefront propagation using the frozen flow hypothesis, since the modes are simply translated across the pupil. In addition, they naturally emerge from the FFT reconstructor, described in Section 5. Fourier modes are the KL modes over a rectangular aperture. The main disadvantage of

Fourier modes is that physically meaningful modes such as tip-tilt, which are often compensated separately, are not easily accessible in Fourier space.

In addition to these modes, the singular modes described in Section 3.1 can be used as a modal basis set.

Fig. 2 shows the first 10 modes for the Zernike, KL and disk harmonic basis sets. It can be seen that the low-order modes are all similar, and the significant differences occur for higher modes.

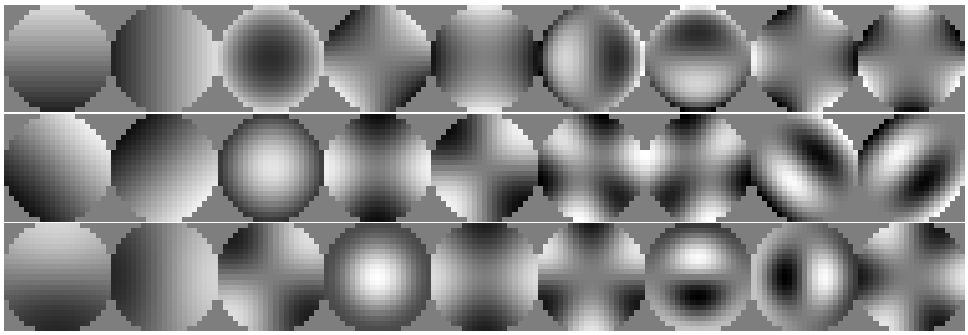

Fig. 2. First 10 modes excluding piston for Zernike (top), Karhunen-Loéve (center) and disk harmonic (bottom) basis sets.

Once we have our modal basis set, we need to calculate the reconstructor. Let $Z = [\mathbf{z_1}^T, \mathbf{z_2}^T, \cdots]$ represent the modes evaluated at the discrete actuator points, such that $\mathbf{a} = Z\mathbf{m}$, where $\mathbf{m}$ is the vector of modal coefficients. The number of columns of Z is equal to the number of modes.

We define a modal interaction matrix, $G_m = G_a Z$, such that

$$\mathbf{s} = G_m \mathbf{m}, \tag{19}$$

and obtain the least-squares solution for the modal coefficients as

$$m = (G_m^T G_m)^{-1} G_m^T s. \tag{20}$$

Because poorly sensed modes, such as piston and global waffle, are not reconstructed, $G_m^T G_m$ is well conditioned.

Generally, the modal coefficients are filtered so that some modes have a higher loop gain than others.[18–20] Let us consider the filtering to be a matrix multiplication by matrix F, which would usually be a diagonal matrix with diagonal values between 0 and 1. Then, using the relationship $a = Zm$, we obtain

$$a = ZF(G_m^T G_m)^{-1} G_m^T s \tag{21}$$

and the reconstructor

$$R = ZF(G_m^T G_m)^{-1} G_m^T. \tag{22}$$

SH WFSs that employ quad cells have an *optical gain* (called the centroid gain) that varies depending on the strength of the turbulence. The same effect occurs for curvature and pyramid sensors, except that the optical gain is not constant but depends on the spatial frequency of the aberrations. As a result, a modal reconstructor with varying modal gains is ideally suited to these sensors.

3.4. *Projection of unwanted modes*

Often, the reconstructor produces unwanted modes. For example, we do not want piston on the DM, and sometimes tip-tilt is corrected with a separate mirror. In this case, we project the unwanted modes from the DM commands. Let us denote the unwanted modes as $\mathbf{v}_i$ and define the matrix V as $V = [\mathbf{v}_1, \mathbf{v}_2, \cdots]$. Then the actuator projection matrix, P_a, is

$$P_a = I - VV^T, \tag{23}$$

and the new reconstructor, R', becomes $R' = P_a R$.

Alternatively (or better still, additionally), certain modes can also be projected out in measurement space. For example, consider tip-tilt measurements from an LGS. These measurements are corrupted by turbulence on the uplink of the laser, and must be removed. The slope projection matrix, P_s, is defined in a manner similar to Eq. (23) and the new reconstructor becomes $R' = RP_s$.

4. Minimum-variance tomographic reconstructors

Tomographic reconstructors are used to convert measurements from several guide stars in to commands for one or more DMs. In this section, we focus on *minimum variance* tomographic reconstructors, which optimally command the DMs to correct the wavefront in the direction of the science targets. This differs from classical reconstructors, which (optimally or otherwise) command the DMs to correct the wavefront in the direction of the WFSs. Minimum-variance reconstructors operate on open-loop measurements and hence require pseudo open-loop control.

Most AO systems with multiple guide stars (GeMS,[4] Argos and LINC-NIRVANA) use classical reconstructors like those presented in Sect. 3. One way to avoid the tomography problem in multi-conjugate adaptive optics (MCAO) is to conjugate the WFSs to each DM, a technique called layer-oriented MCAO.[21,22] Since layer-oriented MCAO also uses classical closed-loop reconstructors, it does not warrant further discussion here. Minimum-variance tomographic reconstructors have been sky-tested on two AO demonstrators: CANARY[23] and RAVEN.[24]

Atmospheric turbulence is distributed vertically in the atmosphere between the ground and an altitude of about 20 km, which means that the turbulence encountered by the science targets and the guide stars depends on their location in the sky. In addition, LGSs emit light from much lower altitudes (typically 10-15 km for Rayleigh guide stars and 90 km for sodium guide stars) than the science targets, giving rise to the well known cone effect (focal anisoplanatism). The problem can be stated as follows: given noisy wavefront sensor measurements, what commands for the DM(s) produce the best correction over the science field? There are two conceptual paradigms to tomographic reconstruction. We either reconstruct virtual turbulence layers at different altitudes (Section 4.1) or we estimate the turbulence in different directions (Section 4.2). Both methods are equivalent, although their computation burdens may differ.

For extremely large telescopes, both the calculation of the reconstructor in soft real-time and the real-time multiplication of slopes by the reconstructor can be computationally challenging. For this reason, a number of alternative approaches that are computationally lighter have been developed and some of these are presented in Section 5.

4.1. *Reconstruction with virtual turbulence layers*

The method of virtual layers has two steps: an estimation step and a fitting step.

- Estimate the wavefront at each layer based on the WFS measurements.
- Project the wavefront onto the DM(s) that optimally corrects the science field.

The details of the reconstruction are comprehensively described in the work of Ellerbroek and his collaborators,[25,26] and their work is outlined (and simplified) here.

Let us assume that the atmospheric turbulence consists of a finite number of very thin layers at different altitudes, h_i, with no turbulence between the layers. The number of layers needed to model the turbulence depends on the diameter of the telescope and the angular extent of the science field and guide stars. The wavefront at each layer is sampled with the same density as the subaperture size or interactuator spacing. Bilinear interpolation is used to evaluate the wavefront in regions between the points where the turbulence is sampled. The wavefront aberration for light passing through point (u, v) in layer h_i is $\psi_i(u, v)$. Let us write as a vector the sampled wavefronts over all of the layers as $x = [\psi_1(u, v), \psi_2(u, v), \cdots]$. This is illustrated in Fig. 3. We want to calculate the estimation matrix, E_x, which produces the best estimate of x given the measurements, s. The relationship between the x and the WFS measurements, s is described by the turbulence influence matrix, G_x:

$$s = G_x x + n. \tag{24}$$

The minimum-variance estimation matrix is:

$$\begin{aligned} E_x &= C_{xs} C_{ss}^{-1} \\ &= \left({G_x}^T C_{nn}^{-1} G_x + C_{xx}^{-1} \right)^{-1} {G_x}^T C_{nn}^{-1}. \end{aligned} \tag{25}$$

This should look familiar as it is the same estimator as Eqs. (13-15). The calculation of C_{xx} is described in Section 4.2.

The second step is to calculate the fitting matrix, which produces the DM actuator commands that best compensate the estimated turbulence: $a = F_x x$. Let us define a vector of residual wavefront errors over the science field as ϕ. Then

$$\phi = H_x x - H_a a, \tag{26}$$

where H_x and H_a are the influence functions that describe how the atmospheric wavefront errors and the DM commands affect the wavefront.

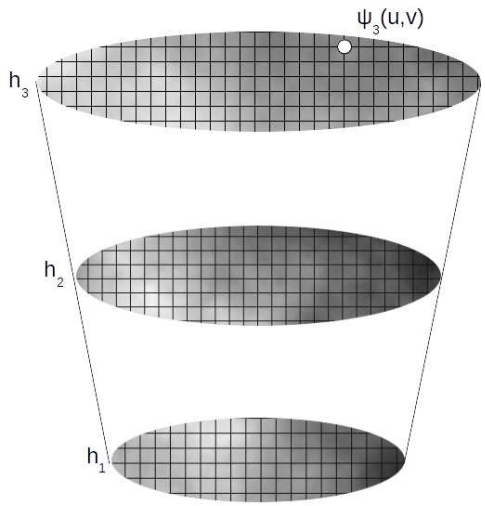

Fig. 3. Schematic of turbulence layers. The grid shows the location of the points where the wavefront is estimated.

The fitting matrix, F_x, is found by minimizing Eq. (26) with respect to a:

$$F_x = ({H_a}^T H_a + \alpha I)^{-1} {H_a}^T H_x. \tag{27}$$

The identity matrix is multiplied by a small constant α to regularize the matrix inversion.

Finally, we obtain the reconstructor as

$$R = F_x E_x. \tag{28}$$

4.2. *Method of spatio-angular covariance matrices*

Instead of estimating the wavefront at different layers, we can estimate the wavefront in different directions.[27–29]

To reconstruct using spatio-angular covariance matrices, we also apply an estimation step followed by a fitting step.

- Estimate the wavefront over each direction of interest in the science field.
- Project the wavefront onto the DM(s) that optimally corrects the science field.

The formulas used are the same, but the definition of the covariance matrices differ.

The estimation step consists of estimating ϕ, the wavefront over every direction in the science field, directly, without explicitly estimating the vertical distribution of turbulence. The minimum-variance estimate for ϕ given the WFS measurements s is:

$$\hat{\phi} = C_{\phi s} C_{ss}^{-1} s. \tag{29}$$

Covariance matrices involving wavefront slopes can be calculated directly.[30] However, we prefer to use covariance matrices involving wavefronts, since the covariances are easier to compute and the associated matrices are smaller.

Let us define the wavefront aberration for light passing through point (u, v) in direction of the WFS i is $\psi_i(u, v)$. We write the sampled wavefronts over all of the different WFS directions as $x = [\psi_1(u, v), \psi_2(u, v), \cdots]$, as shown in Fig. 4. Then

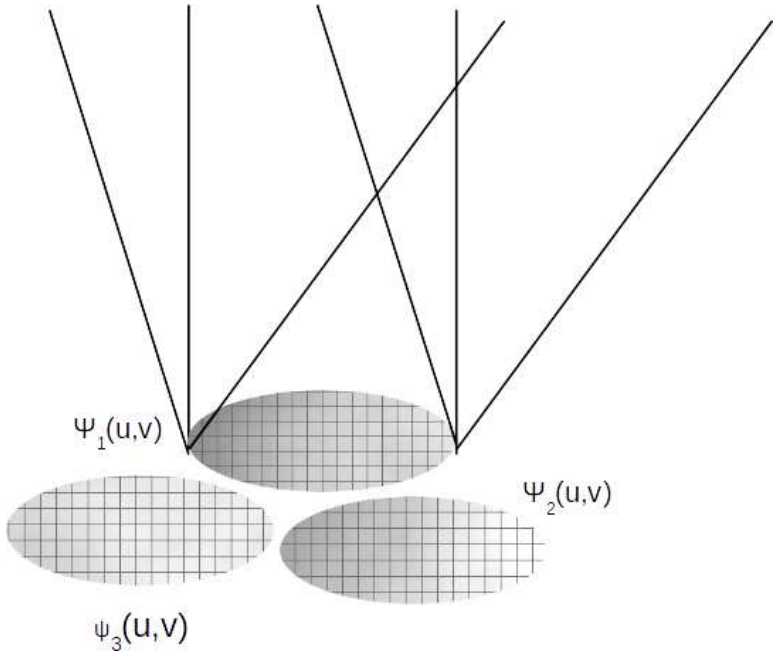

Fig. 4. Schematic of turbulence layers. The grid shows the location of the points where the wavefront is estimated.

$$s = G_x x \tag{30}$$

and the estimation matrix, E_ϕ, can be rewritten as:

$$\begin{aligned} E_\phi &= C_{\phi x} C_{xx}^{-1} C_{xs} C_{ss}^{-1} \\ &= C_{\phi x} C_{xx}^{-1} \left({G_x}^T C_{nn}^{-1} G_x + C_{xx}^{-1} \right)^{-1} {G_x}^T C_{nn}^{-1}. \end{aligned} \tag{31}$$

The fitting matrix, F_ϕ, which converts from wavefront in several different directions onto DM actuator commands, is:

$$F_\phi = ({H_a}^T H_a + \alpha I)^{-1} H_a^T H_\phi. \tag{32}$$

Finally, the reconstructor is given by:

$$R = F_\phi E_\phi. \tag{33}$$

4.3. *Calculation of wavefront covariance matrices*

In this section, we present the formulas for the covariance between two points. These are needed to compute the covariance matrices and hence the reconstructors. These formulas assume von Karman turbulence with a finite outer scale. If the outer scale is infinite (*i.e.*, Kolmogorov turbulence), then the covariance between any two points is infinite and the covariance piston-removed wavefront needs to be calculated.[31]

Let us first consider the covariance of turbulence between two points in the pupil used in Eq. (18). The covariance depends on the distance between the two points, δ_ρ, the outer scale, L_0, and Fried's parameter, r_0, at wavelength λ:[32]

$$\langle \phi(0), \phi^T(\delta_\rho) \rangle = c(2\pi/\lambda)^2 (r_0 f_0)^{-5/3} \left(2\pi f_0 \delta_\rho\right)^{5/6} K_{5/6}\left(2\pi f_0 \delta_\rho\right), \tag{34}$$

where $f_0 = 1/L_0$ and $K_{5/6}$ is the fractional Bessel function of the second kind of order 5/6.

The value of the constant, c, is

$$c = \left(\frac{24}{5}\Gamma\left(6/5\right)\right)^{5/6} \frac{\Gamma(11/6)}{2^{5/6}\pi^{8/3}}, \tag{35}$$

where the symbol Γ represents the gamma function. While this formula appears very complicated, it can be readily programmed and is very useful for calculating covariance matrices.

Next, we consider the covariance of each atmospheric layer in Eq. (25). The turbulence in each layer is completely independent, so the covariance between any two points in layers at different altitudes is zero. The covariance between points within the same layer is given by Eq. (34), but r_0 is replaced with the value corresponding to that layer only, which is

$$r_0(h) = \left[\frac{2.91}{6.88}\left(\frac{2\pi}{\lambda}\right)^2 \sec(\gamma) C_N^2(h)\right]^{-3/5}, \tag{36}$$

where γ is the zenith angle and $C_N^2(h)$ is the turbulence strength at height h.

Finally, we calculate the covariance of the wavefront at two different locations, r_1 and r_2, and in two arbitrary directions, θ_1 and θ_2. We assume that there are N_l layers, each with fraction $\epsilon(k)$ of turbulence at layer k at height $h(k)$. The covariance is:

$$\langle \phi(r_1, \theta_1), \phi^T(r_2, \theta_2) \rangle = c(r_0 f_0)^{-5/3} \sum_{k=1}^{N_l} \epsilon(i) \left(2\pi f_0 \delta_\rho(k)\right)^{5/6} K_{5/6}\left(2\pi f_0 \delta_\rho(k)\right) \tag{37}$$

The distance between two wavefronts at altitude layer k, is

$$\delta_\rho(k) = \left|\rho_1(k) - \rho_2(k)\right|, \tag{38}$$

where

$$\rho_i(k) = (1 - h(k)/z_i) r_i + h(k)\theta_i. \tag{39}$$

The altitude, z_i, is infinite for a natural guide star and a science target, and about 90 km for a sodium guide star.

4.4. *Modal tomographic reconstructors*

The tomographic reconstructors presented thus far are zonal reconstructors. For completeness, we also consider modal tomographic reconstructors. Some of the earliest papers on tomography employed Zernike polynomials as the basis functions.[33–35] The equations to be solved are the same minimum-variance equations, but instead of finding the wavefront at some point in the pupil, we solve for the Zernike coefficients. Zernike polynomials are best suited to circular pupils with a modest order of correction (say 45 modes).

There is one case where modal tomography is essential: tip-tilt tomography. Tip-tilt cannot be accurately measured from LGSs. Instead, tip-tilt measurements are made using one or more NGSs. Let us denote the tip-tilt measurements from the tip-tilt sensors as x. Then the tip-tilt estimate in the desired direction, $\hat{a}$, is given by:

$$\hat{a} = C_{ax} C_{xx}^{-1} x. \tag{40}$$

The cross-covariances for Zernike polynomials can be evaluated using the very long Eq. (32) in Whiteley.[36] Alternatively, it can be calculated using the filter function methodology developed by Sasiela.[37]

5. Alternative implementations of wavefront reconstruction

The only approach to wavefront reconstruction described thus far consists of a reconstructor that is multiplied by a vector of measurements. There are two computational difficulties with this approach for AO systems with a large number of dimensions (*e.g.*, an MCAO system on an extremely large telescope). First, the multiplication of a large matrix with a long vector is computationally demanding ($O(n^2)$, where n is the number of actuators). Second, the computational burden associated with the inversion of matrices with tens of thousands of rows and columns to compute the reconstructor can be even more prohibitive ($O(n^3)$). While the reconstructor matrices do not need to be computed in real time, we require fresh matrices when the atmospheric structure, elevation or telescope pupil change appreciably. In order to avoid both of these issues, a number of different approaches have been proposed.

The fast Fourier transform (FFT) reconstructor[16] replaces the matrix inversion by two FFTs and a mode-by-mode inversion of the Fourier modes. Since FFT operations are $O(n \log(n))$, the computationally load is significantly lower for large values of n. The FFT reconstructor is successfully implemented on the Gemini Planet Imager.[17] An implementation of the tomographic reconstructor using FFTs has also been proposed.[38]

An algorithm called the Cumulative Reconstructor (CuRe) reconstructs the wavefront in $O(n)$.[39] The principle of CuRe is based on the model of the SH WFS data as averaged gradients over the subapertures. With the integration of

the slopes in one dimension, chains of one-dimensional wavefronts estimates are obtained. The independent chains are connected via the general trend (average slopes) in the orthogonal direction. Finally, the chains in both directions are joined to the reconstruction via interpolation. For large numbers of subapertures, domain decomposition is required to reduce the noise propagation of the reconstructor (CuReD).[39] The CuRe algorithm can also be used in conjunction with pyramid sensors by first applying a preprocessing step.[40]

A number of iterative techniques have been proposed to reconstruct the wavefront. Consider, for example, the system of equations corresponding to the single-guide star reconstructor of Eq. (15).

$$a = ({G_a}^T C_{nn}^{-1} G_a + C_{aa}^{-1})^{-1} {G_a}^T C_{nn}^{-1} s. \tag{41}$$

We can write this as:[41]

$$({G_a}^T C_{nn}^{-1} G_a + C_{aa}^{-1}) a = {G_a}^T C_{nn}^{-1} s, \tag{42}$$

where ${G_a}^T C_{nn}^{-1} G_a + C_{aa}^{-1}$ is the left hand side matrix and ${G_a}^T C_{nn}^{-1} s$ is the right hand side matrix. The system of equations can be solved iteratively without inverting any matrices. G_a is a sparse matrix, C_{nn} is a diagonal matrix and C_{aa}^{-1} can be replaced by a sparse approximation[11] or a fractal iterative operator.[41]

Another way to solve the wavefront reconstruction problem iteratively, equivalent to Eq. (41) is to solve first

$$(G_a C_{aa} {G_a}^T + C_{nn}) y = s, \tag{43}$$

for y and then perform the multiplications:

$$a = C_{aa} {G_a}^T y. \tag{44}$$

Using the conjugate gradient algorithm to solve the linear system of equations, a very good approximation to the solution can be attained with a small number of iterations and $O(n)$ operations. A number of papers have been devoted to finding a suitable preconditioner to reduce the number of iterations.[42,43]

Alternatively, the projection of reconstructed wavefronts onto atmospheric layers and fitting these layers onto DMs can be performed using the Kaczmarz algorithm.[44] This uses a similar number of iterations to the conjugate gradient, but each iteration is computationally cheaper. In addition, the matrices do not need to be sparse. The Kaczmarz algorithm appears to be more sensitive to measurement noise.

6. Wavefront Control

In this section, we describe the three types of control loops for astronomical AO systems: closed-loop, open-loop and pseudo open-loop. We then show how to optimize the wavefront control to produce the lowest wavefront error.

6.1. *Control Loop*

The vast majority of astronomical AO systems work in closed-loop. This means that the WFSs measure the *corrected* wavefront, that is, the residual wavefront error after the DM(s) have partially corrected the turbulent wavefront. The simplest and most commonly used closed-loop controller is the integral controller. In the integral controller, the actuator commands at time n, $y[n]$, are updated based on the previous commands, $y[n-1]$ and the current input, $u[n]$:

$$y[n] = y[n-1] + ku[n]. \tag{45}$$

The loop gain k is set to to minimize the residual wavefront error (typically around 0.5). In an AO system, the input is the reconstructed wavefront, $u = Rs$, and the output is the actuator commands, $y = a$. More sophisticated controllers are discussed in Section 6.2.

In open-loop control, the *uncorrected* wavefront is measured by the WFSs, and the command depends only on the reconstructed wavefront:

$$y[n] = u[n]. \tag{46}$$

Closed-loop control has a very important advantage over open-loop control: the details of the AO system, such as the response of the DM and the response of the WFSs, do not need to be known perfectly. An aberration that is only partially corrected the first time will continue to be reduced by successive iterations of the control loop. This means that DM hysteresis or a non-linear response of the DM actuators to an applied voltage are not an issue. In addition, the WFSs only have to be linear and sensitive over a small operating range, which leads to WFSs with small numbers of pixels, such as quad-cell Shack-Hartmann WFSs and pyramid WFSs.

The disadvantage of closed-loop control are that the system can be driven unstable (which could potentially destroy the DMs along with the science exposures) and that a higher frame rate is needed in order to correct the same temporal frequency. A rule of thumb is that the closed-loop control bandwidth (-3 dB bandwidth) is about 5% of the frame rate, while an open-loop system has a control bandwidth of about 30% of the frame rate, as seen in Fig. 5. In order to take advantage of minimum-variance tomographic reconstructors, the turbulence needs to be estimated in open-loop, using open-loop turbulence statistics.[45] However, the system must run in closed-loop. A solution to this problem is to use so-called pseudo-open loop control.[45] Here, the closed-loop measurements, s, are converted into open-loop measurements, s', by adding the wavefront induced by the DM commands, a.

$$s' = s + G_a a. \tag{47}$$

The reconstructor is applied to s', and then the contribution from the DM commands is subtracted to obtain the input u:

$$\begin{aligned} u &= Rs' - a \\ &= R(s + G_a a) - a \\ &= Rs + (RG_a - I)a. \end{aligned} \tag{48}$$

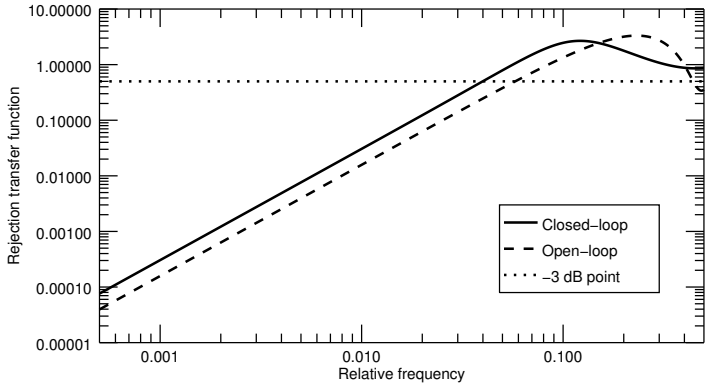

Fig. 5. Typical rejection transfer function in closed-loop (solid) and open-loop (dashed). The dotted line represents the -3 dB point.

Two matrix multiplications are needed to compute the input to the controller. Alternatively, we can convert Eq. (48) to a single matrix multiplication (using a larger matrix):

$$u = \begin{bmatrix} R & RG_a - I \end{bmatrix} \begin{bmatrix} s \\ a \end{bmatrix} \tag{49}$$

The control law for pseudo-open loop control is the same as for closed-loop, *e.g.*, an integral controller described in Eq. (45).

6.2. *Controller Optimization*

Each DM usually has its own controller. A typical AO system will have a tip-tilt loop and a DM loop.

We define a linear controller as one where the new output, $y[n]$, depends linearly on the previous outputs, $y[n-1], y[n-2], \cdots$ and the history of inputs, $u[n], u[n-1], u[n-1], \cdots$. In the z-domain, this is written as

$$Y[z] = \frac{a_0 + a_1 z^{-1} + a_2 z^{-2} + \cdots}{1 + b_1 z^{-1} + b_2 z^{-2} + \cdots}. \tag{50}$$

Here, the values of a_i and b_i are the coefficients of the control law. The integral controller in Eq. (45) has $a_0 = k$ and $b_1 = -1$. In a DM loop, the value of b_1 is set to something like -0.99, in order to "leak" mirror modes that are not well measured by the WFS, such as waffle.

The controller coefficients should be set to minimize the sum (in quadrature) of the bandwidth error (also known as the servo-lag error) and the measurement noise error. This is explained in a seminal paper by Dessenne *et al*[46] with a practical implementation at a telescope described by van Dam *et al.*[8] For high-order controllers, (*i.e.*, linear controllers with many coefficients), the coefficients can be

tailored to the temporal dynamics of the system (such as the compute delay and the temporal response of the DMs) and the disturbance (for example, wind shake and vibrations).[47]

Kalman filters are used to derive optimal control laws is a range of control problems and are also well suited to the AO control problem.[48] They have been successfully implemented on telescopes,[49] particularly to reduce the effects of vibrations.[17] Deriving the Kalman filter involves solving a linear system of equations called the algebraic Riccati equation, the dimensions of which grow very fast with increasing number of equations. As a result, this approach is challenging for the next generation AO systems. The interested reader is referred to a large and growing number of papers on Kalman filters for AO.

References

1. Kasper M, *et al.* Fast calibration of high-order adaptive optics systems. JOSA A. 2004 Jun 1;21(6):1004-8.
2. Meimon S, Petit C, Fusco T. Optimized calibration strategy for high order adaptive optics systems in closed-loop: the slope-oriented Hadamard actuation. Optics Express. 2015 Oct 19;23(21):27134-44.
3. Esposito S, *et al.* High SNR measurement of interaction matrix on-sky and in lab. In SPIE Astronomical Telescopes + Instrumentation. 2006 Jun 14; 62721C.
4. Neichel B, *et al.* Gemini multiconjugate adaptive optics system reviewII. Commissioning, operation and overall performance. Monthly Notices of the Royal Astronomical Society. 2014 May 11;440(2):1002-19.
5. Rigaut FJ, Vran JP, Lai O. Analytical model for Shack-Hartmann-based adaptive optics systems. In Adaptive Optical System Technologies. 1998 Sep 11; 3353:1038-1049.
6. van Dam MA, Lane RG. Wave-front slope estimation. JOSA A. 2000 Jul 1;17(7):1319-24.
7. Gavel DT. Suppressing anomalous localized waffle behavior in least-squares wavefront reconstructors. In SPIE Astronomical Telescopes + Instrumentation. 2003 Feb 1;4839:972-980.
8. van Dam MA, Le Mignant D, Macintosh BA. Performance of the Keck Observatory adaptive-optics system. Applied Optics. 2004 Oct 10;43(29):5458-67.
9. Dekany R, *et al.* PALM-3000: exoplanet adaptive optics for the 5 m Hale telescope. The Astrophysical Journal. 2013 Oct 7;776(2):130.
10. van Dam MA, *et al.* The WM Keck Observatory laser guide star adaptive optics system: performance characterization. Publications of the Astronomical Society of the Pacific. 2006 Feb;118(840):310.
11. Ellerbroek BL. Efficient computation of minimum-variance wave-front reconstructors with sparse matrix techniques. JOSA A. 2002 Sep 1;19(9):1803-16.
12. Kay SM. *Fundamentals of statistical signal processing: estimation theory*, p. 382. Prentice-Hall, New Jersey, (1993).
13. Noll RJ. Zernike polynomials and atmospheric turbulence. JOSA. 1976 Mar 1;66(3):207-11.
14. Dai GM. Modal wave-front reconstruction with Zernike polynomials and KarhunenLove functions. JOSA A. 1996 Jun 1;13(6):1218-25.
15. Milton NM, Lloyd-Hart M. Disk harmonic functions for adaptive optics simulations.

In Adaptive Optics: Methods, Analysis and Applications 2005 Jun 6 (p. AWA3). Optical Society of America.
16. Poyneer LA, Gavel DT, Brase JM. Fast wave-front reconstruction in large adaptive optics systems with use of the Fourier transform. JOSA A. 2002 Oct 1;19(10):2100-11.
17. Poyneer LA, *et al*. Performance of the Gemini Planet Imagers adaptive optics system. Applied Optics. 2016 Jan 10;55(2):323-40.
18. Gendron E, Léna P. Astronomical adaptive optics. 1: Modal control optimization. Astronomy and Astrophysics. 1994 Nov;291:337-47.
19. Gendron E, Léna P. Astronomical adaptive optics. II. Experimental results of an optimized modal control. Astronomy and Astrophysics Supplement Series. 1995 May;111:153.
20. Poyneer LA, Véran JP. Optimal modal Fourier-transform wavefront control. JOSA A. 2005 Aug 1;22(8):1515-26.
21. Arcidiacono C, *et al*. Layer oriented wavefront sensor for MAD on sky operations. In SPIE Astronomical Telescopes + Instrumentation. 2008 Jul 12;70155P-70155P.
22. Farinato J, *et al*. The Multiple Field of View Layer Oriented wavefront sensing system of LINC-NIRVANA: two arcminutes of corrected field using solely Natural Guide Stars. In SPIE Astronomical Telescopes + Instrumentation. 2008 Jul 12; 70155J-70155J.
23. Gendron E, *et al*. MOAO first on-sky demonstration with CANARY. Astronomy & Astrophysics. 2011 May 1;529:L2.
24. Lardière O, *et al*. Multi-object adaptive optics on-sky results with Raven. In SPIE Astronomical Telescopes + Instrumentation 2014 Jul 21 (pp. 91481G-91481G). International Society for Optics and Photonics.
25. Ellerbroek BL. Efficient computation of minimum-variance wave-front reconstructors with sparse matrix techniques. JOSA A. 2002 Sep 1;19(9):1803-16.
26. Ellerbroek BL, Gilles L, Vogel CR. Numerical simulations of multiconjugate adaptive optics wave-front reconstruction on giant telescopes. Applied optics. 2003 Aug 20;42(24):4811-8.
27. Correia C, Jackson K, Vran JP, Andersen D, Lardire O, Bradley C. Static and predictive tomographic reconstruction for wide-field multi-object adaptive optics systems. JOSA A. 2014 Jan 1;31(1):101-13.
28. Conan R, *et al*. The Giant Magellan Telescope laser tomography adaptive optics system. In SPIE Astronomical Telescopes + Instrumentation. 2012 Sep 13; 84473P.
29. Conan R. Fast iterative optimal estimation of turbulence wavefronts with recursive block Toeplitz covariance matrix. In SPIE Astronomical Telescopes + Instrumentation. 2014 Jul 21; 91480R.
30. Vidal F, Gendron E, Rousset G. Tomography approach for multi-object adaptive optics. JOSA A. 2010 Nov 1;27(11):A253-64.
31. Wallner EP. Optimal wave-front correction using slope measurements. JOSA. 1983 Dec 1;73(12):1771-6.
32. R. Conan, "Importance de l'echelle externe pour la Haute Resolution Angulaire en Astronomie," Editions Universitaires Europeennes (2011).
33. Fusco T, *et al.*. Optimal wave-front reconstruction strategies for multiconjugate adaptive optics. JOSA A. 2001 Oct 1;18(10):2527-38.
34. Ragazzoni R, Marchetti E, Valente G. Adaptive-optics corrections available for the whole sky. Nature. 2000 Jan 6;403(6765):54-6.
35. Tokovinin A, Le Louarn M, Viard E, Hubin N, Conan R. Optimized modal tomography in adaptive optics. Astronomy & Astrophysics. 2001 Nov 1;378(2):710-21.
36. Whiteley MR, Welsh BM, Roggemann MC. Optimal modal wave-front compensation for anisoplanatism in adaptive optics. JOSA A. 1998 Aug 1;15(8):2097-106.

37. Sasiela RJ. Electromagnetic wave propagation in turbulence: evaluation and application of Mellin transforms. Springer Science & Business Media; 2012 Dec 6.
38. Gavel DT. Tomography for multiconjugate adaptive optics systems using laser guide stars. InSPIE Astronomical Telescopes + Instrumentation. 2004 Oct 25;1356-1373.
39. Rosensteiner M. Wavefront reconstruction for extremely large telescopes via CuRe with domain decomposition. JOSA A. 2012 Nov 1;29(11):2328-36.
40. Shatokhina I, *et al.* Preprocessed cumulative reconstructor with domain decomposition: a fast wavefront reconstruction method for pyramid wavefront sensor. Applied optics. 2013 Apr 20;52(12):2640-52.
41. Thiébaut E, Tallon M. Fast minimum variance wavefront reconstruction for extremely large telescopes. JOSA A. 2010 May 1;27(5):1046-59.
42. Vogel CR, Yang Q. Fast optimal wavefront reconstruction for multi-conjugate adaptive optics using the Fourier domain preconditioned conjugate gradient algorithm. Optics express. 2006 Aug 21;14(17):7487-98.
43. Gilles L, Ellerbroek BL, Vogel CR. Preconditioned conjugate gradient wavefront reconstructors for multiconjugate adaptive optics. Applied optics. 2003 Sep 10;42(26):5233-50.
44. Rosensteiner M, Ramlau R. Kaczmarz algorithm for multiconjugated adaptive optics with laser guide stars. JOSA A. 2013 Aug 1;30(8):1680-6.
45. Ellerbroek BL, Vogel CR. Simulations of closed-loop wavefront reconstruction for multiconjugate adaptive optics on giant telescopes. Proc. SPIE. 2003 Dec 31; 5169; 206-217.
46. Dessenne C, Madec PY, Rousset G. Optimization of a predictive controller for closed-loop adaptive optics. Applied optics. 1998 Jul 20;37(21):4623-33.
47. Agapito G, *et al.* Frequency based design of modal controllers for adaptive optics systems. Optics Express. 2012 Nov 19;20(24):27108-22.
48. Kulcsár C, Raynaud HF, Petit C, Conan JM, de Lesegno PV. Optimal control, observers and integrators in adaptive optics. Optics express. 2006 Aug 21;14(17):7464-76.
49. Sivo G, *et al.* First on-sky SCAO validation of full LQG control with vibration mitigation on the CANARY pathfinder. Optics express. 2014 Sep 22;22(19):23565-91.